Deliverable 2.2: Tunability of the Hex-SiGe bandgap.

1. Introduction

The band structure of hexagonal SiGe has been calculated by the Jena group and will be presented in deliverable 1.3. In short, the Jena group has calculated the SiGe band structure for a different ratios of Si and Ge atoms in an 8-atom unit cell and for all the different orderings of the atoms in the unit cell. The results of these calculations are shown as data points in figure 1b. As a guide to the eye coloured bands are shown marking the spread of the energy bands. In Fig. 1a the averages of these energy bands are plotted, showing that Hex-SiGe is predicted to be a direct bandgap semiconductor for Ge-compositions above 65%. The figure also shows a broad tunability of the direct bandgap from 0.31 eV up to the crossing point with the L-band at 0.72 eV, which would correspond to a wavelength of 1.7 µm. It should be mentioned that the calculated band structure data correspond to low temperature.

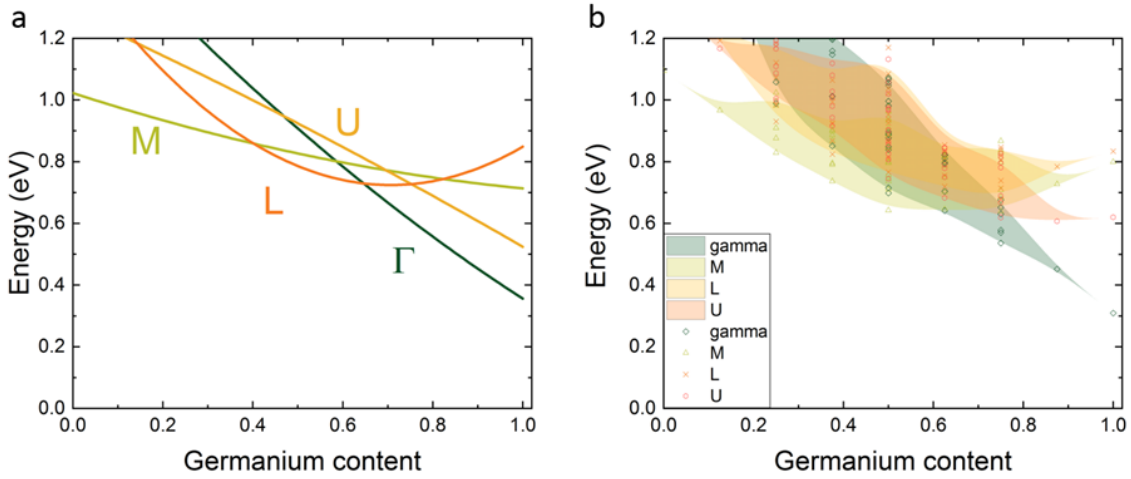

Figure 1. *(a) Averages of the calculated band edges as a function of the Ge-composition for Hex-SiGe. (b) Calculated band edges for the different configurations of Si and Ge within the unit cell.*

2. Growth of Hex-SiGe nanowire shells

Here, we present the details of the growth process of hexagonal the $Si_{1-x}Ge_x$ crystals throughout the whole range of stoichiometry of the alloy. The hexagonal crystal phase of the $Si_{1-x}Ge_x$ crystal is achieved via the "Crystal Transfer" technique reported in[1,2,3] where the hexagonal crystal structure of the $Si_{1-x}Ge_x$ is adopted from a hexagonal material template. In our project, this is achieved by utilizing non-tapered and single-crystalline wurtzite $GaAs$ nanowires that act as a template and then overgrow them with an epitaxial layer of $Si_{1-x}Ge_x$ using Metal Organic Vapor Phase Epitaxy (MOVPE). A schematic illustration for the full growth process is shown in **Figure. 2**.

The GaAs NWs are grown by the Vapor-Liquid-Solid (VLS) mechanism utilizing gold (Au) catalyst seeds. The Au catalyst seeds were deposited in nano disks arrays arrangement on a $GaAs\ (111)_B$ substrate via the electron beam lithography technique. The growth template in **Figure. 2a** is brought to the MOVPE reactor. Then, the gas precursors needed to grow the GaAs core NWs (Trimethyl Gallium ($TMGa$) and Arsine (AsH_3)) are introduced to the growth chamber as illustrated in **Figure. 2a**. After

[1] Algra R E, et al., Crystal Structure Transfer in Core / Shell Nanowires *Nano Lett.* **11**, 1690–4 (2011)
[2] Hauge H.I.T. et al., Hexagonal Silicon Realized *Nano Lett.* **15,** 5855–60 (2015)
[3] Hauge H.I.T. et al., Single-Crystalline Hexagonal Silicon Germanium *Nano Lett.* **17**, 85−90 (2017)

the GaAs NWs are grown (see, **Figure. 2b**), they are chemically treated to remove the Au droplets (see, **Figure. 2c**) to avoid gold contamination. Eventually, the GaAs core is used as hexagonal material template to grow the $Si_{1-x}Ge_x$shell by introducing the suitable gas precursors of the shell growth (Germane (GeH_4) and Disilane (Si_2H_6)) in the reactor, see **Figure. 2d**.

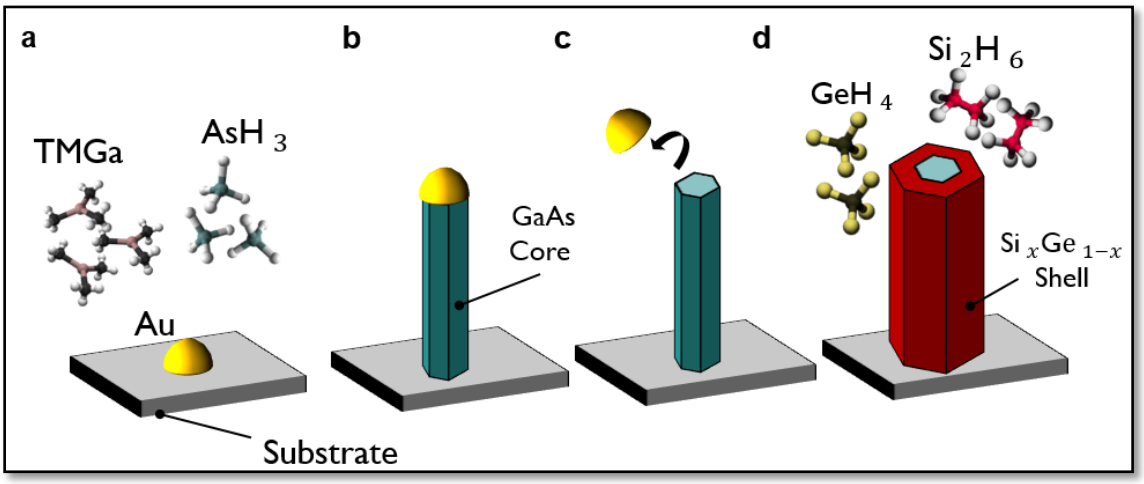

***Figure 2**. **Schematic Illustration of the Nanowires Growth Process:** explaining that the growth starts with (a) A substrate patterned with Au catalyst seeds and the gas precursors are introduced in the MOVPE reactor, by time and as the growth proceeds (b) Au-catalysed GaAs core nanowires are grown, the (c) Au seeds are chemically etched from the GaAs cores, and eventually (d) A $Si_{1-x}Ge_x$ shell is epitaxially grown around the GaAs cores.*

Figure. 3 shows representative 30°-titled Scanning Electron Microscopy (SEM) images for the GaAs core NWs with a diameter of 50 nm, and a full range of stoichiometry of $Si_{1-x}Ge_x$ with a shell thickness of around 250 nm. The indicated label percentages in the SEM images are the Ge percentage in the shells. We have substantially improved the growth of our Hexagonal $Si_{1-x}Ge_x$nanowire shells. We also successfully managed to grow a big volume of these shells with a very high crystalline quality which was, to our knowledge, never presented before.

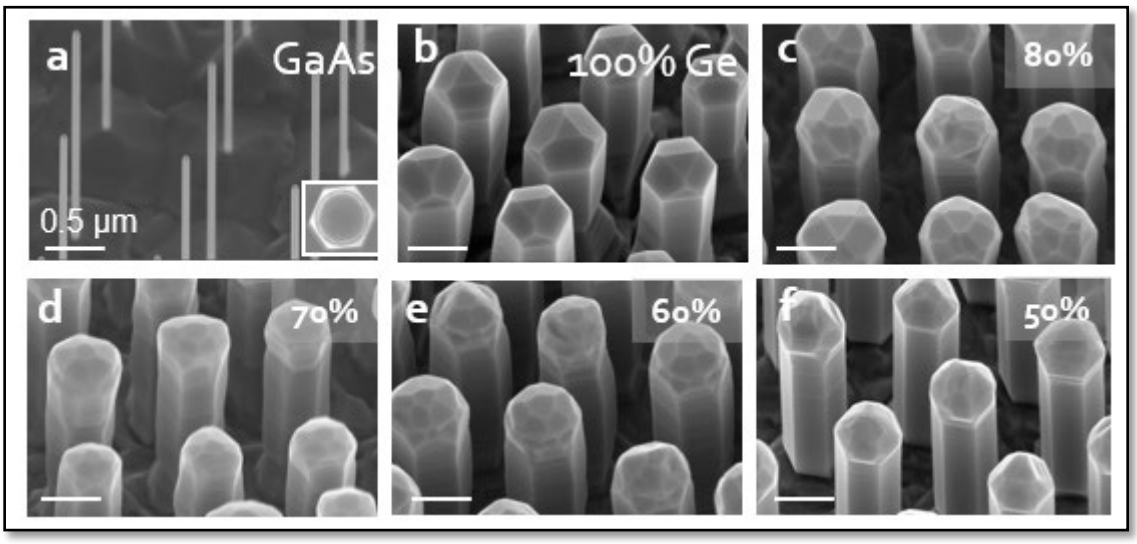

***Figure 3**. Representative 30-degree tilted SEM images of (a) Wurtzite GaAs core nanowires, and hexagonal (b) 100% Ge, (c) $Si_{02}Ge_{0.8}$, (d) $Si_{0.3}Ge_{0.7}$, (e) $Si_{0.4}Ge_{0.6}$, and (f) $Si_{0.5}Ge_{0.5}$shells grown around the GaAs core nanowires presented in (a). The scale bar is 0.5 µm and the indicated label percentages are the Ge content in the shells.*

The high crystalline quality is presented in **Figure. 4** by showing high resolution High Angular Annular Dark Field Scanning Electron Microscope (HAADF-STEM) images of a pure hexagonal Ge (**Figure. 4a**) and high silicon content $Si_{0.63}Ge_{0.37}$ (**Figure. 4b**) nanowire shells. The characteristic *ABAB*… stacking of the hexagonal phase is visible in the images, confirming the hexagonal crystal phase.

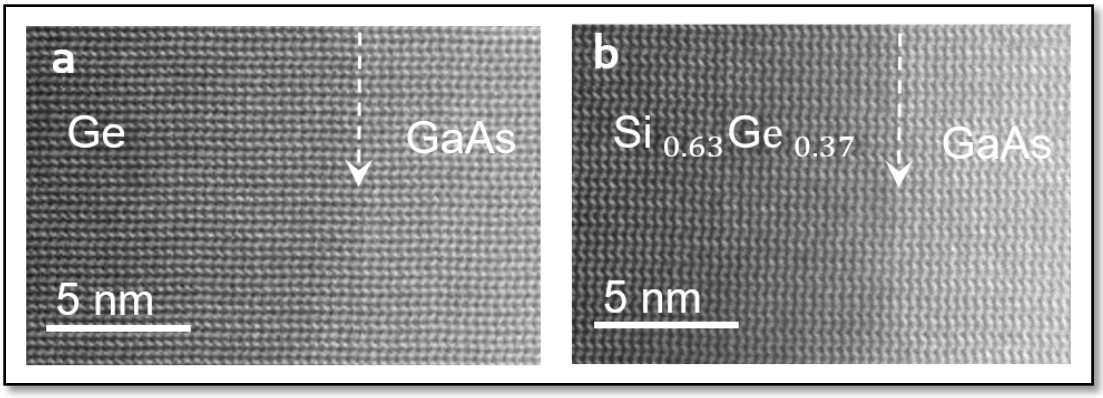

Figure 4. *High resolution HAADF-STEM images of the crystal structure of (a) 100% Ge, and (b)* $Si_{0.63}Ge_{0.37}$ *confirming the hexagonal crystal structure. The white arrows are guides for the eye to indicate the interface between the wurtzite GaAs nanowire cores and the shells.*

3. Determination of the Ge-composition by Energy Dispersive X-ray Spectroscopy

We subsequently measured the Si- and the Ge-content in the Hex-SiGe shells by Energy Dispersive X-ray Spectroscopy (EDS) within a Transmission Electron Microscopy (TEM) setup. These measurements allow to measure the compositions spatially dependent as shown in **Figure 5c,d** and to unambiguously relate the measured compositions to the Hex-SiGe shell which is visible in **Figure. 5b**.

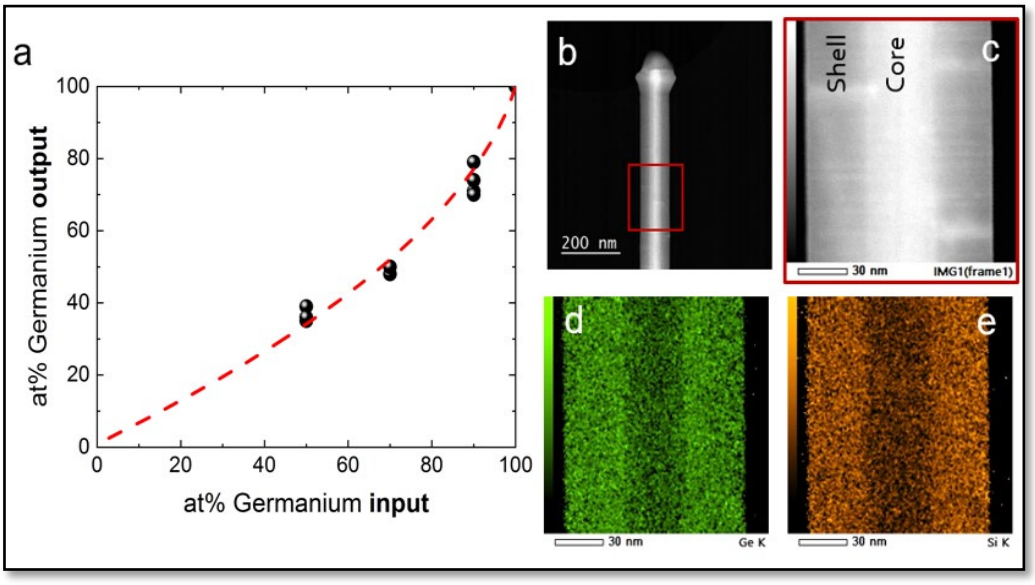

Figure 5. SiGe Composition calibration: *(a) A plot of the input Si-content by using the Si and Ge fluxes within the MOVPE with the output Si-composition as measured by EDS. (b) TEM picture of the core-shell nanowire. 2D EDS maps of (c) Si and (d) Ge.*

Figure. 5a is showing the resulting calibration of the measured output Si composition as a function of the ratio of the input fluxes during MOVPE growth. We will use the parabolic fit (indicated as a red dashed line) to assign the proper composition to all Hex-SiGe shells we have measured. To confirm

composition uniformity across the hexagonal volume of the SiGe shells, Atom Probe Tomography (APT) characterization has been performed. APT is based on the evaporation of atoms in the form of ions from a single nanowire by means of an electric field or laser pulsing. Single nanowires are picked up by means of an electron focused ion beam (FIB) and fixed on a tip-shaped sample as depicted in the SEM image in **Figure. 6a**. Ions are projected from the tip apex onto a position-sensitive single ion detector by the electric field. On the basis of the measured positions and the time-of-flight between the tip apex and the detector surface a 3D reconstruction of the analyzed volume is created. We have analyzed a $Si_{0.23}Ge_{0.77}$ SiGe shell volume radially, across the diameter of the core shell of the nanowire and axially, across the length of the nanowire, as explained in the schematic illustration of **Figure. 6b**. The radial profile (in **Figure. 6c**) is performed across a 900 nm core/shell diameter and the axial profile (in **Figure**. **6d, e**) analysis is integrated over the full length of the wire 1.1 µm. The profiles confirms the uniformity of the composition in the volume of the shell.

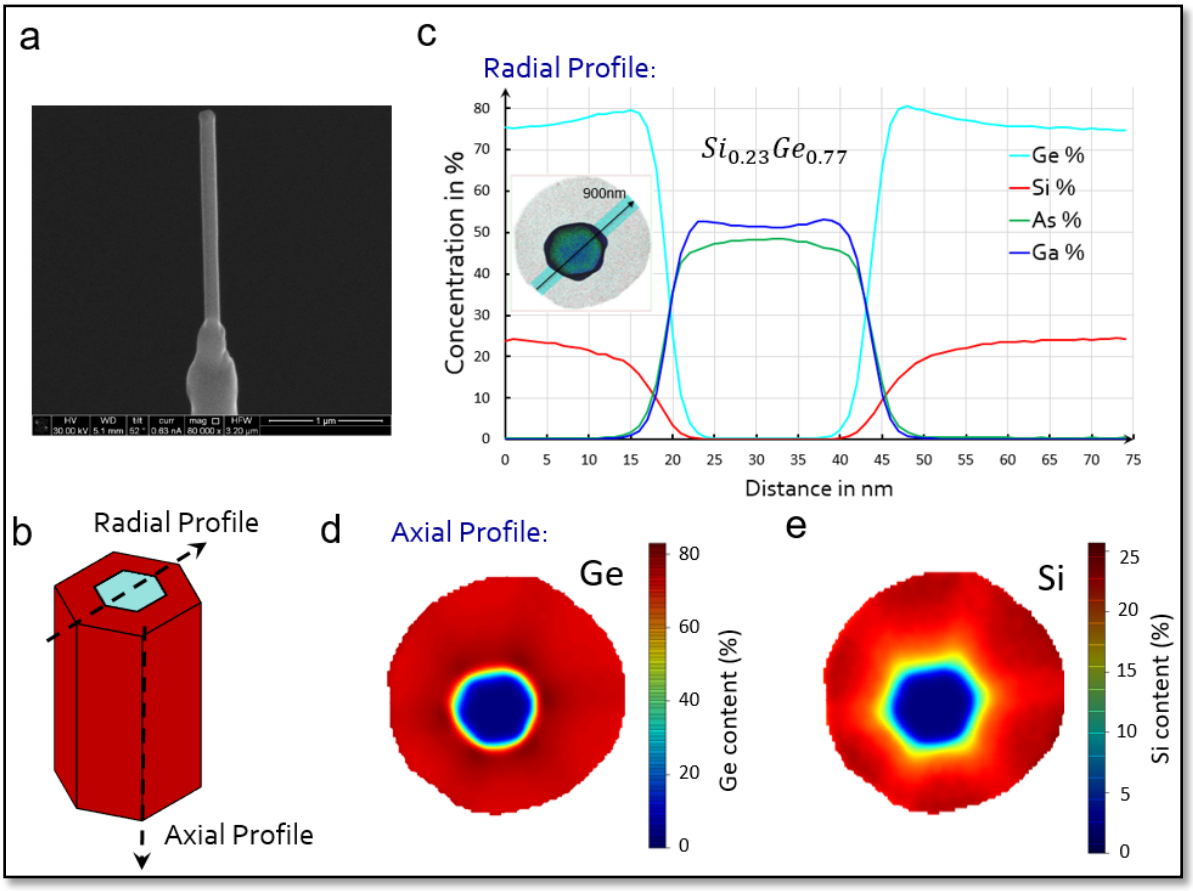

***Figure 6**: Atom Probe Tomography Characterization: **(a)** A Hex-$Si_{0.23}Ge_{0.77}$ /GaAs core/shell nanowire, **(b)** Schematic illustration of the characterized structure with guiding arrows to the extracted profiles explained in (c) and (d). **(c)** A radial profile across the diameter of the nanowire displaying the elemental composition of the core/shell structure, **(d), (e)** Axial profiles across the length of the nanowire viewing the Ge and Si composition in the axial direction, respectively. Both profiles confirm the SiGe composition uniformity in the nanowire, radially and axially.*

4. Tunability of the bandgap for Hex-SiGe

We performed step-scan Fourier Transform Infrared Spectroscopy (SS-FTIR) measurements to measure the low-temperature photoluminescence spectra of our improved Hex-SiGe nanowire shells. The samples were excited with a 976 nm laser with an excitation density of about 2 kW/cm^2 at a temperature of 4K. We studied samples which were grown with different atomic input percentages of

germanium when grown in the reactor. The compositions in growth were subsequently converted into the real compositions by using the calibration graph presented in **Fig. 5**. The tunability of the emission spectrum of Hex-SiGe over a wide wavelength range from< 2.0 µm up to 3.5 µm is experimentally demonstrated in **Fig. 7**.

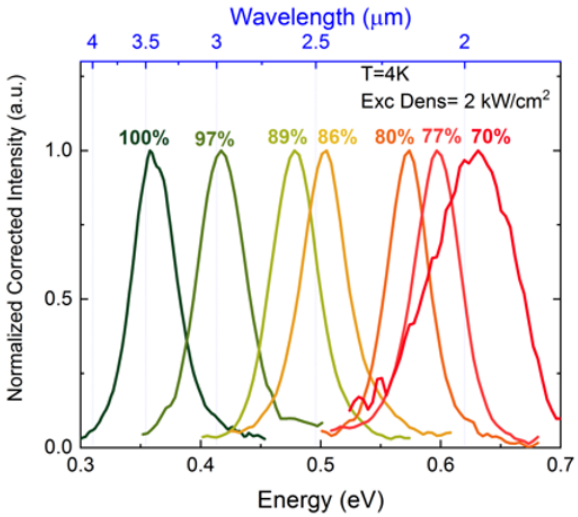

Fig. 7: *Photoluminescence spectra of core-shell GaAs-$Si_{1-x}Ge_x$ nanowires taken at a temperature of 4K and an excitation density of 2 kW/cm² for different Ge-compositions.*

We note that the our Hex-SiGe nanowire shells feature different broadening mechanisms. Firstly, one may assume that the shell composition is not entirely uniform. We however observe a very clear energy shift between the 86% Ge sample and the 89% Ge sample, indicating that we are able to accurately choose the composition with only minor compositional fluctuations across the nanowire shell. Compositional variations translate into alloy broadening in spectroscopy. A second argument against the alloy broadening mechanism is that alloy broadening is expected to vary with the Ge-concentration as *x(1-x)* and is expected to be absent for Hex-Ge. Except for the 70% Ge sample, we do not observe a strong variation of the full width at half maximum (FWHM) with Ge-composition, thus providing a strong indication that compositional variations are not responsible for the observed broadening.

The observed spectral broadening is most probably due to the n-type doping of the Hex-SiGe shell due to the evaporation of As from either the surface of the substrate or the wall of the MOVPE reactor during growth. We measured the As-doping composition by using atom probe tomography and obtained an As-doping concentration of $2.10^{19}/cm^3$ for the present generation of samples, indicating that the individual donor atoms have merged into a donor band which has in turn merged with the conduction band continuum. We thus expect a metallic like behavior of our present generation of Hex-SiGe nanowire shells, which will be visible as band filling due to the Burnstein-Moss effect. This band filling effect results in the broadened emission spectra we presently observe. The As-doping also explains why we do not observe discrete recombination peaks due to donor-related or exciton-related optical transitions. The high doping concentration implies that we observe transition between the lowest Γ_8 conduction band and either the uppermost Γ_9 valence band or alternatively to acceptor levels slightly below the Γ_9 valence band due to Ga impurities originating from the GaAs. Since the acceptor binding energy is expected to be ~30 meV, which is relatively low compared to the optical transition energy, we can approximately attribute the observed transition energies as the fundamental bandgap of the Hex-SiGe alloys.

Subsequently, we compare our experimental data for the fundamental bandgap with the theoretical calculations as performed by the Jena group in **Fig. 8**. We observe an excellent agreement between theory and experiment for the direct bandgap Hex-SiGe samples with a Ge-composition above 75%. For the samples with lower Ge-composition, our experimental data seem to closely match the calculated band edge energies of the lowest energy atomic configurations. Assuming that all different atomic configurations are present within our Hex-SiGe material, we expect that the charge carriers will quickly diffuse towards the lowest bandgap region, i.e. towards the lowest energy atomic configuration.

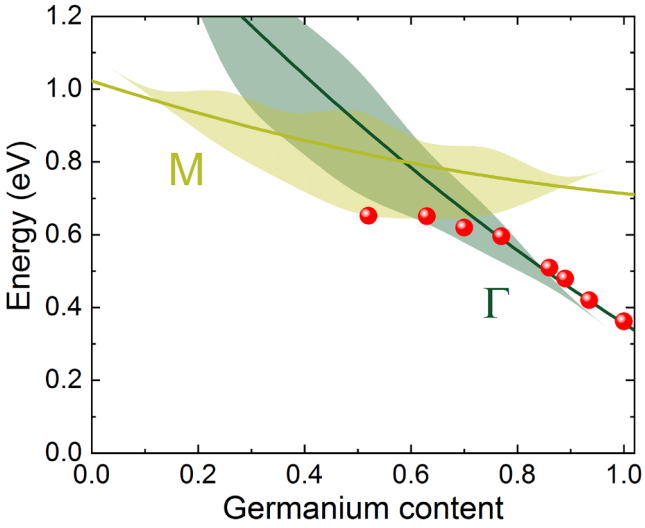

***Fig. 8**: Comparison of the position of our experimentally measured photoluminescence spectra with the colored bands introduced in Fig. 1 that represent the band edges for the different atomic configurations.*

With the assumption that the charge carriers quickly diffuse towards the lowest bandgap atomic configurations, we observe an excellent agreement between theory and experiment. The very good agreement with theory provides strong evidence for the direct bandgap character of the Hex-SiGe emission for Ge-compositions above approximately 75%.

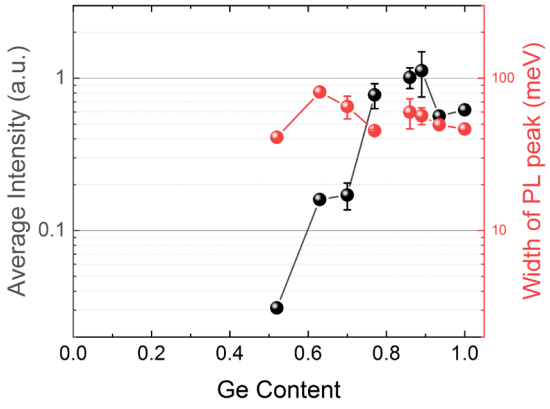

***Fig. 9**: Measured integrated photoluminescence intensities versus the Ge-content in Hex-SiGe shells.*

The data in **Fig. 8** do show excellent agreement between theory and experiment, but the graph is not showing the influence of the direct-indirect transition on the integrated photoluminescence intensity. We plot the integrated intensities in **Fig. 9** where the PL of all the samples was measured using the same MCT detector. The measured intensities are thus comparable. The important conclusion from

Fig. 9 is that direct bandgap Hex-SiGe shows an appreciable larger amount of photoluminescence than indirect Hex-SiGe at a Ge-content of 0.5. One might think that the decrease of the PL intensity is due to an increasing amount of lattice mismatch between the WZ GaAs core and the Hex-SiGe shell. However, an increasing amount of lattice mismatch would first be visible as an increase of the broadening of the photoluminescence peak. Such increasing broadening is clearly not observed in the data of **Fig. 9**.

5. **Evidence for band-to band emission.**

For the interpretation of the results, it is important to study the power dependent photoluminescence at 4K. These data are presented in **Fig. 10**.

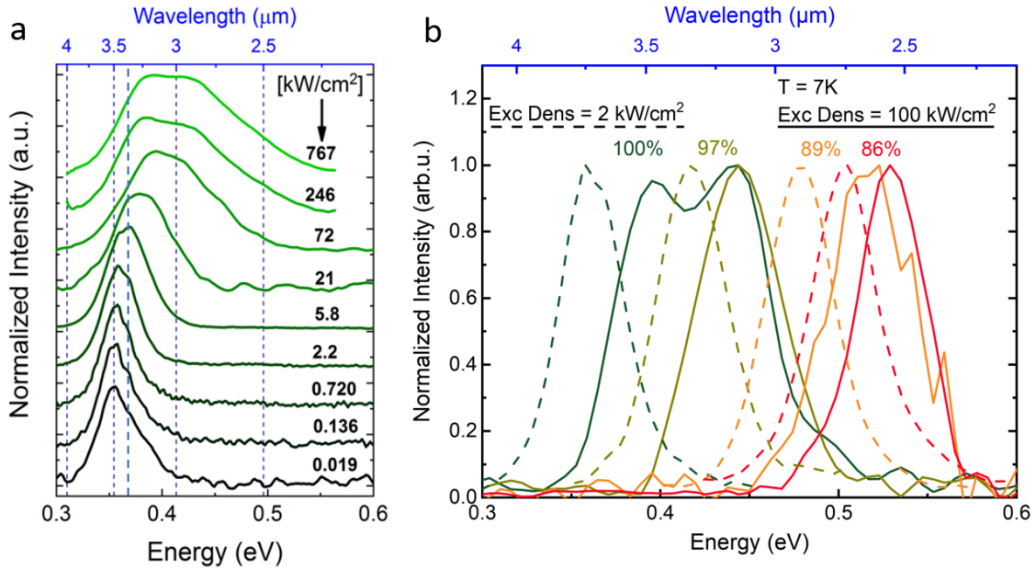

Fig. 10: (a) Excitation power dependence of the photoluminescence at 4K of hexagonal Ge shells grown around a WZ GaAs nanowire core showing a bandfilling behavior.

It is shown in **Fig. 10a** that we observe a strong bandfilling effect which is also known as the Burnstein-Moss shift. It is clear that at higher excitation, the peak starts to broaden at the high energy side due to bandfilling. This type of broadening is typically observed for a band-to-band transition at high excitation. The observation of a Burnstein-Moss shift is thus a clear indication of the direct bandgap character of Hex-SiGe. We also measured the bandfilling behavior for Hex-SiGe down to 86% Germanium content as shown in **Fig. 10b**. In this graph, the low excitation density measurements are plotted as dashed lines.

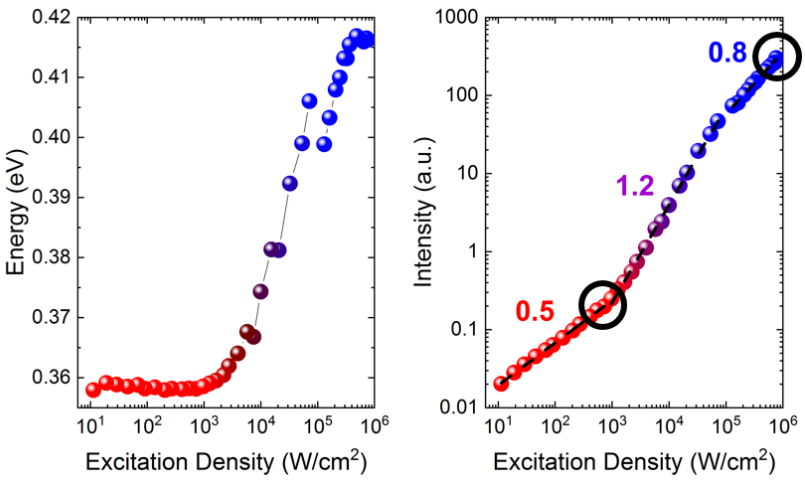

Fig. 11: Excitation power dependence of (a) the peak energy and (b) the emission intensity of Hex-Ge at 4K.

When studying the peak power dependence in **Fig. 10**, we observe a first peak at 0.35 eV and a second peak at 0.37 eV. As soon as the second peak starts to take over, we observe a continuous blue shift of the emission peak due to the Burnstein-Moss effect as shown in **Fig. 11a**. At approximately the same excitation density, the slope of the emission intensity versus excitation power changes from 0.5 to 1.2 as shown in **Fig. 11b**. The slope can be understood[4] by the fact that the photoluminescence emission intensity can be expressed as $I_{PL} \sim Bn^2$ and

$$I_{Excitation} \sim I_{total\ recombination} \sim An + Bn^2 + Cn^3 \sim a{I_{PL}}^{1/2} + bI_{PL} + c{I_{PL}}^{3/2},$$

with A the coefficient for Shockley Read Hall (SRH) nonradiative recombination, B the coefficient for radiative recombination and C the coefficient for nonradiative Auger recombination. We thus expect a slope of unity for radiative recombination, a slope of 2 for e.g. surface recombination and a slope of 2/3 for Auger recombination. At low temperature, the electron-acceptor transition is proportional to $nA^{(0)}$ and is expected[5] to provide a slope close to ½. The small slope of 0.5 thus indicates that we probably observe the donor band to acceptor level transition $e\text{-}A^{(0)}$ due to e.g. neutral Ga acceptors. We expect to observe this small slope until all Ga-acceptors are ionized, which is happening at an excitation density above ~1kW/cm^2. In this regime, we observe a slope of 1.2 which indicates primarily radiative band-to-band recombination together with SRH recombination which raises the slope above unity. This explanation is supported by **Fig. 11a** which is showing a clear Burnstein-Moss shift starting above ~1kW/cm^2 It is an important observation that radiative recombination seems to remain dominant up to an excitation density of 10^5/cm^2. For even higher excitation density, the slope decreases towards 0.8, which can be explained by either heating effects or to the addition of Auger recombination with an expected slope of 2/3. Heating effects are also observable in **Fig. 10** by the increasing tail of the Fermi-Dirac distribution of the charge carriers. We conclude that our present generation of Hex-SiGe nanowire shells is capable to generate direct bandgap band-to-band recombination for excitation densities between 1 and 100kW/cm^2. We expect lasing to be possible in this regime, provided that the cavity quality factor can be made high enough.

[4] S. R. Johnson, D. Ding, J.-B. Wang, S.-Q. Yu, and Y.-H. Zhang, Excitation dependent photoluminescence measurements of the nonradiative lifetime and quantum efficiency in GaAs, Journal of Vacuum Science & Technology B25, 1077 (2007)
[5] T. Schmidt, K. Lischka and W. Zulehner, Excitation-power dependence of the near-band-edge photoluminescence of semiconductors, Phys. Rev. B45 (16) (1992)

6. Observation of room temperature emission

Looking back into the history of many III/V semiconductors, most materials initially showed a very small PL efficiency at room temperature. Subsequent materials development has improved the room temperature photoluminescence efficiency by e.g. proper surface passivation or improvements in the crystal growth. The measured temperature dependence of the Hex-Ge emission spectrum is shown in **Fig. 12**. It is quite remarkable that room temperature emission, which is technologically of upmost importance, is already observed in unpassivated samples at "relatively low" excitation density of 1.8 kW/cm^2.

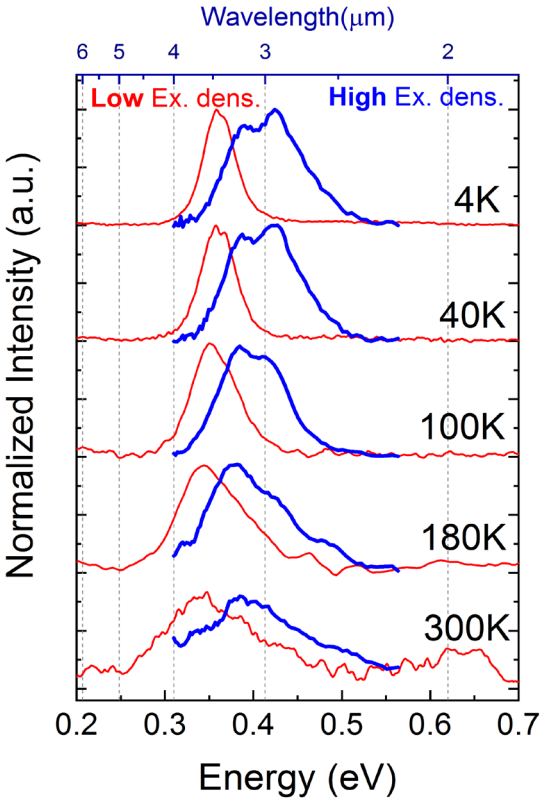

Fig. 12: Temperature dependence of the photoluminescence spectrum of Hex-Ge.

The room temperature photoluminescence emission intensity can be quantified by measuring the ratio of the integrated PL intensity at 4K and at 300K. Since it is usually assumed that the internal quantum efficiency (IQE) for the emission of photoluminescence is 100% at 4K, this ratio provides the IQE at room temperature. In the case of Hex-Ge, we observe that the integrated PL at 300K is still 5% of the PL emission at 4K, as shown in **Fig. 13**. (Should be worked out better. Our IQE at 4K is not 100%.)

The observed photoluminescence spectra show a shape which loosely resembles the product of the density of states in a bulk semiconductor $(\sim\sqrt{E})$ multiplied with a Fermi-Dirac distribution, which exhibits the expected broadening with temperature. The only disturbing fact is the observation of a tail below 0.3 eV at T>300K, which is not yet understood. The peak at 0.65 eV is due to cubic Ge which is deposited in between the nanowires as well as near the top of each nanowire due to a small amount of axial growth during the intended growth of the Hex-Ge shell. The important message we obtain from the T-dependent photoluminescence spectra is that the observed spectral shape is again providing evidence for a band-to-band recombination which remains observable up to room temperature.

At an high excitation of 770 kW/cm^2, we observe large bandfilling at low temperature. At increasing temperature, the amount of bandfilling is decreasing due to an increasing amount of nonradiative (surface) recombination. At high temperature, the amount of bandfilling is reduced but the thermal broadening of the Fermi-Dirac distribution is more dominant.

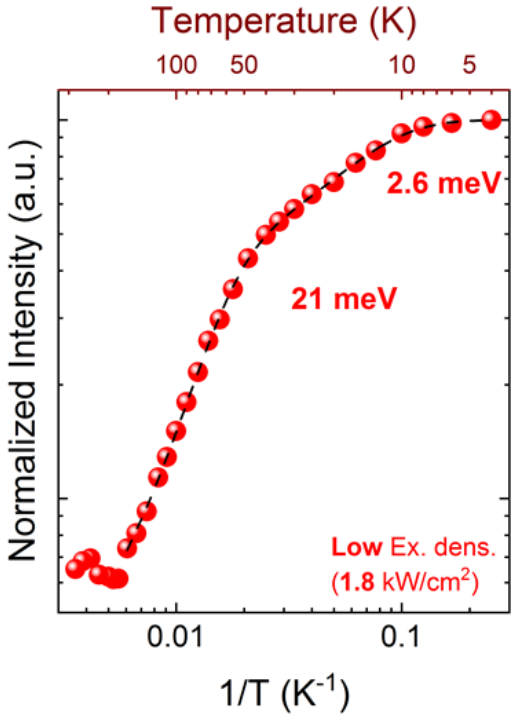

Fig. 13: Ratio of the integrated PL between 300K and 4K, showing a relatively large photoluminescence intensity at 300 K which is still 5% of the low-temperature emission intensity.

Fig. 13 shows the activation energies by plotting the integrated photoluminescence intensity versus the inverse temperature. We obtain activation energies of 2.6 meV and 21 meV at low excitation, which might correspond to the donor and acceptor binding energies. The experimental observation that the integrated PL efficiency only decreases by a factor 20 when increasing the temperature between 4K and 300K might be partially explained by the high unintentional n-doping due to As, which will partially saturate possible electrons traps and which will increase the radiative recombination through the factor $I_{PL}{\sim}B(n+\Delta n)(p+\Delta p)\approx n\Delta p$ in which n=2.10^{19}/cm^2. The high n-doping will of course also increase nonradiative Auger recombination, in particular through the "eeh" process in which the excess energy of the electron before recombination is transferred to another electron. The influence of Auger processes will be a subject of further investigation.

7. **Measurement of the photoluminescence lifetime**.

Theoretical calculations on Hex-Ge indicate a transition matrix element for the Γ_8-Γ_9 transition which is a factor 10^4 smaller than for a typical III/V semiconductor. Fortunately, the transition matrix element become much larger for hex-SiGe as shown in deliverable 1.3. For achieving lasing in Hex-Ge, the n.p product should thus be 10^4 larger than in GaAs, or implying that both the electron and hole concentrations should be 100x larger. This is not impossible to achieve since the amount of bandfilling will increase when the amount of radiative recombination is decreased. We expect that a typical Hex-Ge light emitter will operate at a higher amount of bandfilling than a conventional group III/V light emitter. The theoretical predictions for Hex-SiGe are more positive. In addition, a large amount of

bandfilling is easier to achieve a very small volume of e.g. a nanowire shell, provided that other mechanisms like Auger recombination are not dominant. The other option is to apply lattice strain in order to shift the fully allowed Γ_7 band edge closer towards the Γ_8 band edge, which is expected to convert Hex-SiGe into a direct bandgap semiconductor with a large transition matrix element. The final possibility is that the calculated matrix elements can be enhanced by k-non-conservation by e.g. defects or the nanowire surface. We are setting up a photoluminescence lifetime setup using a superconducting single photon detector (SSPD) capable to detect single photons with a wavelength around 2 µm. With this setup, we expect to be capable to measure the radiative lifetime of Hex-SiGe in the near future.

8. Conclusions
    - The very good agreement between experiment and theory provides strong evidence for the direct bandgap character of the Hex-SiGe emission for Ge-compositions above approximately 75%.
    - Experimental demonstration of direct bandgap tunability from 3.5 µm to < 2.0 µm by tuning the Ge content.
    - Direct bandgap Hex-SiGe shows an appreciable (50x) larger amount of photoluminescence than indirect bandgap Hex-SiGe
    - The observation of a Burnstein-Moss shift is a clear indication of the direct bandgap character of Hex-SiGe.
    - Our present generation of Hex-SiGe nanowire shells is capable to generate direct bandgap band-to-band recombination for excitation densities between 1 and 100kW/cm^2. We expect lasing to be possible in this regime, provided that the cavity quality factor can be made high enough.
    - The observed spectral shape of our temperature-dependent photoluminescence spectra is providing additional evidence for a band-to-band recombination.
    - Even in unpassivated samples, technologically important room temperature emission is already observed at a relatively low excitation density of 1.8 kW/cm^2 using a moderately sensitive MCT detector.
    - The relative efficient room temperature emission is evidenced by an integrated PL efficiency which decreases by less than a factor 20 when increasing the temperature between 4K and 300K.